

# Characterizing High-Quality High-Dimensional Quantum Key Distribution by State Mapping Between Different Degrees of Freedom

Fang-Xiang Wang,<sup>1,2,3</sup> Wei Chen,<sup>1,2,3,\*</sup> Zhen-Qiang Yin,<sup>1,2,3,†</sup> Shuang Wang,<sup>1,2,3</sup>  
Guang-Can Guo,<sup>1,2,3</sup> and Zheng-Fu Han<sup>1,2,3</sup>

<sup>1</sup>*CAS Key Laboratory of Quantum Information, University of Science and Technology of China, Hefei 230026, China*

<sup>2</sup>*Synergetic Innovation Center of Quantum Information & Quantum Physics, University of Science and Technology of China, Hefei, Anhui 230026, China*

<sup>3</sup>*State Key Laboratory of Cryptology, P.O. Box 5159, Beijing 100878, China*

(Received 25 September 2018; revised manuscript received 31 December 2018; published 27 February 2019)

Quantum key distribution (QKD) guarantees the secure communication between legitimate parties with quantum mechanics. High-dimensional QKD (HDQKD) not only increases the secret key rate but also tolerates higher quantum bit error rate (QBER). Many HDQKD experiments have been realized by utilizing orbital-angular-momentum (OAM) photons as the degree of freedom (DOF) of OAM of the photon is a prospective resource for HD quantum information. In this work, we propose that a high-quality HDQKD based on polarization-OAM hybrid states can be realized by utilizing state mapping between different DOFs and we characterize this HDQKD. Both the preparation and measurement procedures of the proof-of-principle verification experiment are simple and stable. Our experiment verifies that a  $0.60\% \pm 0.06\%$  QBER and a  $1.849 \pm 0.008$ -bit secret key rate per sifted signal can be achieved for a four-dimensional QKD with the weak coherent light source and decoy state method.

DOI: 10.1103/PhysRevApplied.11.024070

## I. INTRODUCTION

Higher-order Poincaré (HOP) has recently been introduced to describe the total angular momentum of a photon [1,2]. Photons with orbital angular momentum (OAM) [3] are also called twisted photons [4]. The poles of the HOP are scalar vortex states and can be expressed as a product of polarization and OAM. The polarization of a scalar vortex is spatially homogeneous. The states on the HOP except the poles are nonseparable polarization-OAM hybrid states and are named vector vortices [5–9], which are spatially polarized. The Poincaré sphere, typically used to describe polarization states, has also been introduced to describe the degree of freedom (DOF) of OAM, where the basis states are two orthogonal OAM states [10]. The Hilbert space of OAM is infinite theoretically and photons with more than 10 000 quanta OAM have been realized in experiment [11]. Thus, the DOF of OAM of the photon is a prospective high-dimensional (HD) resource for classical optical communication [12–18] and quantum information [4,19], such as HD quantum entanglement [20], quantum memory [21], quantum teleportation [22], and quantum key distribution (QKD) [23,24]. QKD [25] guarantees the secure communication of two parties with quantum physics [26].

The traditional QKD protocols, distributing a 1-bit raw key per effective detection issue, have been rapidly developed in past decades [27–31]. HDQKD not only increases the secret key distribution rate but also makes the legitimate parties better able to detect an eavesdropper than the traditional two-dimensional QKD does [32–34]. Hence, HDQKD with OAM photons has been a hot topic in recent years [35–44].

On the other hand, polarization is one of the most mature DOFs in classical and quantum communication. By combining both Poincaré spheres of polarization and OAM, the HOP is able to describe polarization-OAM hybrid vector vortices. Owing to the nonseparable characteristic, the polarization and OAM of the vector vortex state on the HOP can be manipulated by each other. The nonseparable characteristic also reveals the unique feature of the spatially polarized structure of the vector vortex [5–8].

In this work, by using the nonseparable feature of the vector vortex, we realize the state mapping between the DOF of OAM and polarization. Then, a proof-of-principle characterization experiment is implemented to verify the feasibility of a four-dimensional QKD. By taking advantage of the state mapping method between different DOFs, only polarization manipulation to a vector vortex state on the HOP is necessary to implement the HDQKD. Thus, the preparation and measurement fidelities are determined by

\*weich@ustc.edu.cn

†yinzq@ustc.edu.cn

the polarization control procedure, which has a high precision. We propose that a HDQKD system based on our protocol could achieve a  $1.849 \pm 0.008$ -bit secret key rate per sifted signal (SKRPSS) with an ultralow quantum bit error rate (QBER) of  $0.60\% \pm 0.06\%$  and ultrahigh stability.

## II. PROTOCOL

The vector vortex state on the equator of the HOP is in the form of  $|L\rangle| -l \rangle + e^{i\theta}|R\rangle|l\rangle$  and is completely spatially polarized, where  $|L\rangle$  ( $|R\rangle$ ) is the left (right) circular polarization and  $|l\rangle$  is the OAM with  $l\hbar$  quantum number. Such a vector vortex can be prepared by the Sagnac loop structure with a spiral phase plate [2,45] or a  $q$  plate [46–48], among which the  $q$ -plate method is easier to realize [23, 48,49]. A  $q$  plate can be expressed as  $\hat{Q}(q) = (|L\rangle\langle R|) \otimes (\sum_l |l-2q\rangle\langle l|) + (|R\rangle\langle L|) \otimes (\sum_l |l+2q\rangle\langle l|)$ , where  $2q$  is the quantum number of OAM and is determined by the  $q$  plate. As the Hilbert space of OAM is not closed, the summation of the  $q$  plate is also not closed, in principle. For a linear polarized input Gaussian beam, the output state from the  $q$  plate is  $|\mathcal{V}\rangle = \hat{Q}(q)|H\rangle|0\rangle = (1/\sqrt{2})(|R\rangle|2q\rangle + |L\rangle|-2q\rangle)$ . It is a radial polarized vector vortex [see Fig. 1(a)] on the equator of the HOP. If we project the state into homogeneous linear polarization, then  $\hat{P}_s(\alpha)|\mathcal{V}\rangle = (e^{-i\alpha}/2)(\cos\alpha|H\rangle + \sin\alpha|V\rangle)(|2q\rangle + e^{2i\alpha}| -2q\rangle)$ , where  $\hat{P}_s(\alpha) = (\cos\alpha|H\rangle + \sin\alpha|V\rangle)(\cos\alpha|H\rangle + \sin\alpha|V\rangle)$  is the projector,  $\alpha$  is the projection angle, and the subscript  $s$  means that the manipulation is operated on the DOF of polarization. The projective state becomes a product state of polarization and OAM. Figure 1(a) gives the beam profiles of the radial polarized vector vortex prepared by a  $q$  plate with  $q = 1$ . By rotating the projection angle  $\alpha$ , the projective polarization state rotates on the equator of the polarization Poincaré sphere and the projective OAM state rotates on the equator of the OAM Poincaré sphere [10] simultaneously, although we have not manipulated the state in the DOF of OAM directly. Thus,

we only need to operate on a single DOF to fulfill the manipulation of multiple DOFs. For example, by applying another unitary transform  $\hat{U}_s(\alpha)$  in the DOF of polarization after the projector, the state becomes  $\hat{U}_s(\alpha_2)\hat{P}_s(\alpha_1)|\mathcal{V}\rangle = (e^{-i\alpha_1}/2)[\cos(\Delta\alpha)|H\rangle + \sin(\Delta\alpha)|V\rangle](|2q\rangle + e^{2i\alpha_1}| -2q\rangle)$ , where  $\Delta\alpha = \alpha_2 - \alpha_1$ , and the unitary transform  $\hat{U}_s(\alpha)$  is given by

$$\hat{U}_s(\alpha) = \begin{pmatrix} \cos\alpha & \sin\alpha \\ \sin\alpha & -\cos\alpha \end{pmatrix}.$$

Then, by choosing  $\alpha_1, \Delta\alpha \in \{0, \pi/2\}$  and  $\alpha_1, \Delta\alpha \in \{\pi/4, -\pi/4\}$ , two sets of four-dimensional mutually unbiased bases (MUBs)  $\{|\psi_i\rangle\}$  and  $\{|\phi_i\rangle\}$  are constructed, respectively.  $\{|\psi_i\rangle\}$  and  $\{|\phi_i\rangle\}$  are defined as

$$\begin{aligned} |\psi_1\rangle &= |H\rangle(|2q\rangle + | -2q\rangle), |\psi_2\rangle = |H\rangle(|2q\rangle - | -2q\rangle), \\ |\psi_3\rangle &= |V\rangle(|2q\rangle - | -2q\rangle), |\psi_4\rangle = |V\rangle(|2q\rangle + | -2q\rangle), \\ |\phi_1\rangle &= |D\rangle(|2q\rangle + i| -2q\rangle), |\phi_2\rangle = |D\rangle(|2q\rangle - i| -2q\rangle), \\ |\phi_3\rangle &= |A\rangle(|2q\rangle - i| -2q\rangle), |\phi_4\rangle = |A\rangle(|2q\rangle + i| -2q\rangle), \end{aligned} \quad (1)$$

where  $|D(A)\rangle = \frac{1}{\sqrt{2}}(|H\rangle \pm |V\rangle)$ . Figures 1(b1)–(b4) and Figs. 1(c1)–(c4) give the beam profiles of  $\{|\psi_i\rangle\}$  and  $\{|\phi_i\rangle\}$ , respectively. Only polarization control is necessary for the MUBs' preparation procedure. The MUBs' preparation procedure [Fig. 2(a)] can be realized with high-speed devices because  $\hat{P}_s(\alpha_1)$  can be factorized by  $\hat{P}_s(\alpha_1) = \hat{U}_s(\alpha_1)\hat{P}_s(0)$  [see Fig. 2(b)]. By applying this factorization, only two active unitary transforms  $\hat{U}_s(\alpha_1)$  and  $\hat{U}_s(\alpha_2)$  are necessary for the MUBs' preparation procedure. The MUBs can then be generated with high speed by realizing  $\hat{U}_s(\alpha_1)$  and  $\hat{U}_s(\alpha_2)$  with electro-optical modulators (EOMs). Then, the MUBs in Eq. (1) can be constructed by choosing  $\alpha_1, \alpha_2 \in \{0, \pi/2\}$  and  $\alpha_1, \alpha_2 \in \{\pi/4, -\pi/4\}$ , respectively.

Previously, we have proposed the preparation of two sets of four-dimensional MUBs by utilizing the nonseparable feature of vector vortices. Another important part of

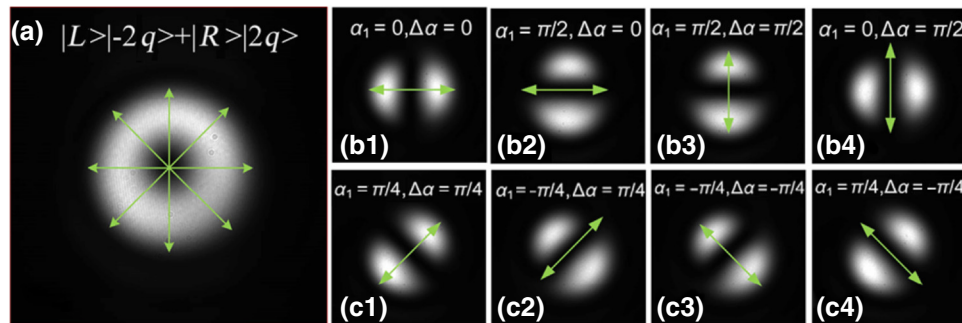


FIG. 1. The experimental realized beam profiles of (a) the radial vector vortex and the corresponding MUBs (b1)–(b4)  $\{|\psi_i\rangle\}$  and (c1)–(c4)  $\{|\phi_i\rangle\}$  constructed in Eq. (1). The beam profiles are prepared by a  $q$  plate with  $q = 1/2$ . The green arrows are the orientation of the linear polarization.

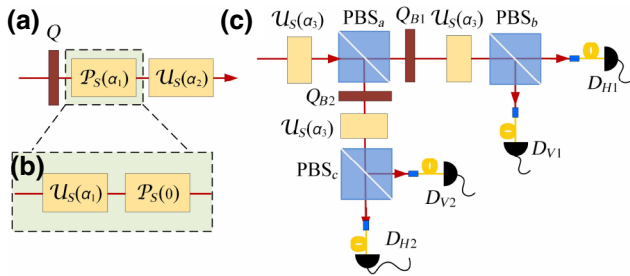


FIG. 2. The schematic setups of preparation and projective measurement of two sets of four-dimensional MUBs: (a) the preparation procedure, (b) the factorization of  $\hat{P}_s$ , and (c) the projective measurement setup.  $Q$ ,  $Q_{B1(B2)}$  are the  $q$  plates;  $D_{H(V)}$  is the single-photon detector.

a QKD system is the complete projective measurement of these MUBs. Now, we construct the complete projective measurement setup as below.

A  $q$  plate can manipulate both DOFs of polarization and OAM [as shown by  $\hat{Q}(q)$ ]. According to this property of the  $q$  plate, we propose a simple setup to convert the OAM projection to polarization projection [see Fig. 2(c)] and realize the high-precision complete projective measurement for the prepared MUBs. In Fig. 2(c), the unitary transform  $\hat{U}_s(\alpha_3)$  is used to choose the projective basis from  $\mathcal{M}_1 = \sum_i |\psi\rangle_i \langle \psi|$  ( $\alpha_3 = 0$ ) and  $\mathcal{M}_2 = \sum_i |\phi\rangle_i \langle \phi|$  ( $\alpha_3 = \pi/4$ ). Without the loss of generality, we take  $\mathcal{M}_1$  as an example.  $\hat{U}_s(\alpha_3)$  becomes a unit matrix. The first polarizing beam splitter (PBS<sub>a</sub>) realizes the projective measurement of polarization. Then two  $q$  plates ( $Q_{B1}$  and  $Q_{B2}$ ) are used to twist the polarization and OAM:

$$\begin{aligned} \hat{Q}_{B1}|H\rangle(|2q\rangle + e^{2i\alpha_1}| -2q\rangle) &= (1/\sqrt{2})[|L\rangle + e^{2i\alpha_1}|R\rangle]|0\rangle \\ &\quad + |R\rangle|4q\rangle + e^{2i\alpha_1}|L\rangle|-4q\rangle], \\ \hat{Q}_{B2}|V\rangle(|2q\rangle + e^{2i\alpha_1}| -2q\rangle) &= (1/\sqrt{2})[| -L\rangle + e^{2i\alpha_1}|R\rangle]|0\rangle \\ &\quad + |R\rangle|4q\rangle - e^{2i\alpha_1}|L\rangle|-4q\rangle]. \end{aligned} \quad (2)$$

According to Eq. (2), the input OAM state  $|2q\rangle + e^{2i\alpha_1}| -2q\rangle$  has been mapped to the polarization state  $|L\rangle + e^{2i\alpha_1}|R\rangle$  with zero OAM. By ignoring the nonzero OAM terms, the input state can be discriminated by polarization projection now. Thus, by cascading a PBS (PBS<sub>b</sub> and PBS<sub>c</sub>) and a single-mode fiber (SMF) in each path, we project  $|\psi\rangle_1$ ,  $|\psi\rangle_2$ ,  $|\psi\rangle_3$  and  $|\psi\rangle_4$  to the single-photon detectors (SPDs)  $D_{H1}$ ,  $D_{V1}$ ,  $D_{H2}$ , and  $D_{V2}$ , respectively, while  $|\phi\rangle_i$  projects to all SPDs with equal probabilities. The SMFs are used to filter out all nonzero OAM terms, which thus leads to a 50% efficiency loss. A similar conclusion can be obtained for the projective basis  $\mathcal{M}_2$ . Hence, we realize the complete projective measurement of the two sets of four-dimensional MUBs by utilizing the “twist”

ability of  $q$  plates. Our projective measurement method possesses high resolution as the extinction ratio of polarization projective measurement is much higher than the directly OAM projective measurement.

### III. PROOF-OF-PRINCIPLE EXPERIMENT

Without the loss of generality, a proof-of-principle experiment has been implemented to verify the feasibility of a four-dimensional BB84-protocol QKD [25] (as shown in Fig. 3), where Alice prepares and transmits the states to Bob through the quantum channel and Bob makes projective measurements to the received states. In the state preparation procedure of Alice, the light source is a Ti:sapphire locked pulsed laser. The wavelength of the laser is  $780 \pm 5$  nm, the pulse width is within 200 fs, and the repeating rate is 77 MHz.  $\hat{U}_s(\alpha_1)$  and  $\hat{U}_s(\alpha_2)$  are realized by half-wave plates (HWPs) [HWP<sub>1</sub> and HWP<sub>2</sub> in Fig. 3(a)]. The light intensity is attenuated to the single-photon level by attenuators (Att1 and Att2) before being transmitted to Bob. The attenuators are also used to realize the “vacuum + weak decoy state” method [27,28,50]. The average photon numbers of the transmitted signal and decoy states are  $\mu \simeq 0.053$  and  $\nu \simeq 0.017$ , respectively. In the projective measurement procedure of Bob, the chosen basis  $\hat{U}_s(\alpha_3)$  is realized by HWPs [HWP<sub>3</sub> and HWP<sub>4</sub> in Fig. 3(b)]: the rotation angles of HWP<sub>3</sub> and HWP<sub>4</sub> are zero for  $\mathcal{M}_1$  and  $\pi/8$  for  $\mathcal{M}_2$ , respectively. A 3.05-ns time delay is used to multiplex the transmissive and reflective signals of PBS3 to the following identical path after PBS4. SMFs are used to project the zero OAM terms into single-photon detectors (SPDs, SPCM-AQRH-14 of Excelitas Technologies Corp.). The detection efficiency and dark count rate of the SPD are 60% and 67 Hz, respectively. The time resolution of the SPD is 350 ps with full width at half maximum (FWHM).

We use a time-to-digital converter (TDC) with 50-ps time resolution to detect the arrival time of photons

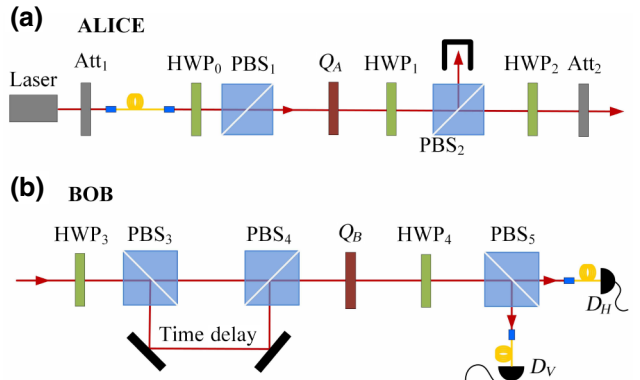


FIG. 3. Experimental setup of the HD-QKD. (a) The state preparation setup of Alice. (b) The projective measurement setup of Bob.  $Q_A$ ,  $Q_B$  are the  $q$  plates; “Att” is the optical attenuator.

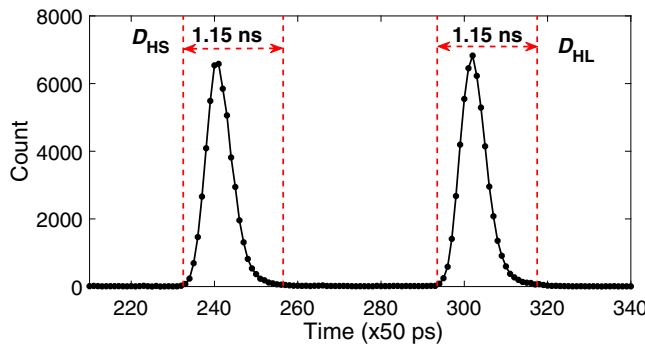


FIG. 4. The arrival time distribution of the SPD  $D_H$  in Fig. 3(b).

through the short and long paths of Bob. Figure 4 gives the detection results of  $D_H$  in Fig. 3(b). According to the time distribution of count events, the effective detection window of the SPDs is set to 1.15 ns with postselection by the TDC. Figure 4 shows that a 3.05-ns time delay is sufficient for time resolution between the short and long paths. The effective dark count rate for the postselection detection window is then  $7.7 \times 10^{-8}$  per pulse.

The projective measurement results of Bob's setup for transmitted signal states are shown in Fig. 5. The results show very low crosstalk as all diagonal elements are larger than 0.99. We define projective efficiency  $\mathcal{E} = 1 - e_b$  to evaluate the projective quality, where  $e_b$  is the QBER of the projective measurement of a transmitted state. For example,  $e_b = \sum_{i \neq 1} i \langle \psi | \psi \rangle_1$  for  $|\psi\rangle_1$ . The projective efficiencies of signal and decoy states are shown in Table I. The projective efficiencies are all larger than 99%. The maximum measurement errors are as low as  $3\sigma_{\mu_{\max}} \simeq 0.07\%$  and  $3\sigma_{v_{\max}} \simeq 0.10\%$  for the signal and decoy states, respectively. According to Table I, the average QBERs of the signal and decoy states are  $e_\mu \simeq 0.60 \pm 0.06\%$  and  $e_v \simeq 0.65 \pm 0.10\%$ , respectively.

According to the Gottesman-Lo-Lütkenhaus-Preskill formula [28,51] for HDQKD [32], the secret key rate of the  $d$ -dimensional BB84-QKD can be estimated by

$$\mathcal{R} \geq q_m Q_\mu \{-f_{\text{EC}}(e_\mu) H_d(e_\mu) + \Delta_1 [\log_2 d - H_d(e_1)]\}, \quad (3)$$

where  $q_m$  depends on the QKD protocol and is 1/2 in our experiment;  $Q_\mu$  and  $e_\mu$  are the gain and QBER of the signal state, respectively;  $\Delta_1$  is

TABLE I. The projective efficiency  $\mathcal{E}$  and measurement error  $3\sigma$  (three times the standard deviation) of the projective measurement setup.

	$ \psi\rangle_1$	$ \psi\rangle_2$	$ \psi\rangle_3$	$ \psi\rangle_4$	$ \phi\rangle_1$	$ \phi\rangle_2$	$ \phi\rangle_3$	$ \phi\rangle_4$
$\mathcal{E}_\mu$	99.35%	99.32%	99.42%	99.68%	99.19%	99.73%	99.16%	99.33%
$3\sigma_\mu$	0.05%	0.06%	0.05%	0.04%	0.06%	0.04%	0.07%	0.06%
$\mathcal{E}_v$	99.27%	99.24%	99.41%	99.67%	99.13%	99.64%	99.12%	99.31%
$3\sigma_v$	0.10%	0.10%	0.09%	0.07%	0.11%	0.08%	0.13%	0.10%

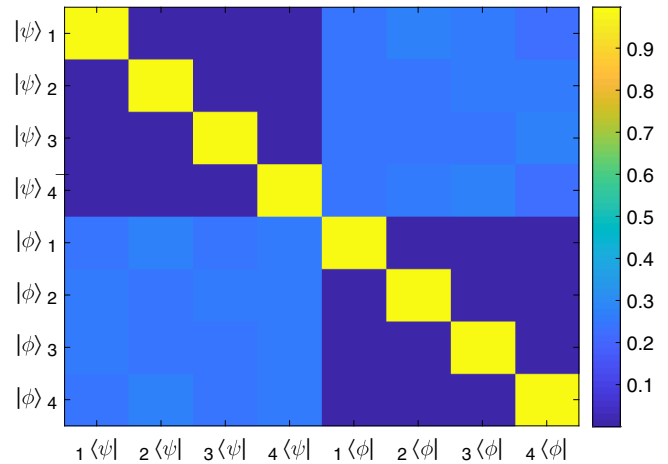


FIG. 5. The probability distribution of the projective measurement setup for transmitted signal states with  $\mu \simeq 0.053$ .

the fraction of single-photon signals transmitted by Alice;  $f_{\text{EC}}(e_\mu)$  is the error correction efficiency of the signal state; and  $H_d(e_\mu) = -(1 - e_\mu) \log_2(1 - e_\mu) - e_\mu \log_2[e_\mu/(d - 1)]$  is the  $d$ -dimensional Shannon entropy. By applying the “vacuum + weak decoy state” method [50],  $\delta_1$  and  $e_1$  can be estimated by the following constraint inequalities:  $\Delta_1 \geq [\mu^2 e^{-\mu}/(\mu v - v^2)] \{(Q_v/Q_\mu)e^v - (v^2/\mu^2)e^\mu - [(\mu^2 - v^2)/\mu^2](Y_0/Q_\mu)\}$ ,  $Y_1^{L,v,0} = [\mu/(\mu v - v^2)] \{Q_v e^v - (v^2/\mu^2)Q_\mu e^\mu - [(\mu^2 - v^2)/\mu^2]Y_0\}$  and  $e_1 \leq e_v Q_v e^v - e_0 Y_0 / Y_1^{L,v,0} v$ , where  $Y_0$  is the dark count rate of the SPD;  $e_0$  is the QBER of the vacuum state; and  $Q_v$  and  $e_v$  are the gain and QBER of the weak decoy state, respectively. The corresponding parameters of our experiment are  $\mu \simeq 0.053$ ,  $v \simeq 0.017$ ,  $Q_\mu \simeq 4.03 \times 10^{-3}$ ,  $Q_v \simeq 1.33 \times 10^{-3}$ ,  $e_\mu \simeq 0.60 \pm 0.06\%$ ,  $e_v \simeq 0.65 \pm 0.10\%$ ,  $Y_0 \simeq 8 \times 10^{-8}$ , and  $e_0 = 0.5$ . Then, we obtain the calculated SKPSS  $\mathcal{R}/(q_m Q_\mu) \simeq 1.849 \pm 0.008$ , where we have set  $f_{\text{EC}}(e_\mu) = 1$  [the SKPSS is about 1.840 bits by considering a practical error correction efficiency  $f_{\text{EC}}(e_\mu) = 1.15$ ].

#### IV. DISCUSSION

According to the experimental results, the QBER and the corresponding error of our experiment are very low  $e_\mu \simeq 0.6 \pm 0.06\%$ . This value is a result of the state preparation and measurement methods proposed here. For both

state preparation and measurement procedures, we successfully map OAM superposition state manipulation into polarization manipulation. As polarization manipulation technologies are mature and have high precision, our protocol achieves very low QBER. Furthermore, the mapping procedures apply no interferometric structure [e.g., the Mach-Zehnder interferometer (MZI)] and make the system stable (the experimental error is less than 0.1%). It should be addressed that, although the laser repetition rate is 77 MHz, the QBERs of different transmitted states are measured one by one by rotating the HWPs manually in our proof-of-principle experiment.

A performance comparison of HDQKD systems based on OAM photons is shown in Table II, where we list some key indexes of HDQKD systems. The QBER of ours is the lowest and, thus, the corresponding SKRPSS is much higher than that of other four-dimensional systems. Although the authors of Ref. [42] achieved a higher SKRPSS of 2.05 bits, it is a seven-dimensional QKD system with 10.5% QBER.

The commonly used tools for OAM state preparation are the spatial light modulator (SLM), the  $q$  plate, and the digital micromirror device (DMD) [4,19,48]. The main disadvantage of these tools is the relatively low generation speed (from 10 Hz to several kHz [42]). By combining with other means such as the multipath encoding method, the generation speed difficulty can be overcome. However, these means are still complex. For example, the high-generation-rate method of Ref. [37] requires two cascading MZIs. The state generation rate of our method can achieve 100 MHz by replacing HWP1 and HWP2 in Fig. 3(a) with free-space EOMs. The free-space EOM requires high half-wave voltage and is difficult to run with higher modulation rate. Although there is still a long way to go to make them practical, the integrated optical waveguides [52] and modulators [53,54] may be a potential solution to high-speed modulation of OAM photons.

The OAM and polarization-OAM state measurements are usually carried out by the hologram-based OAM filter [19,55], the interferometric method [56,57], the  $q$ -plate method with wave plates [48], and the geometric transformation method [58–61]. The hologram-based OAM filter lacks efficiency. The geometric transformation method can fulfill the projective measurement of tens of OAM modes simultaneously. However, the crosstalk between adjacent modes is still a little higher [60] for high-quality QKD systems (see Refs. [38,39,41,42,62] in Table II). The  $q$ -plate method used in previous works is actually the mode filter [35,40,48]. By mapping the OAM projection into the polarization projection, we achieve a high-precision complete projective measurement of polarization-OAM hybrid states with a much simpler setup. It should be emphasized that only comparing with the QBER and SKRPSS of HDQKD systems in Table II is not rigorous in a sense because the photon sources, encoding states, and

TABLE II. Secret key rate comparison of some typical OAM-based HDQKD works with our works.  $d$  is the dimensionality of the QKD system. WCS is the weak coherent laser source; a dash indicates a value not shown in the reference; PPKTP and BBO represent the single-photon sources generated by the spontaneous parametric-down-conversion process with periodically poled potassium titanyl phosphate and barium borate nonlinear crystals, respectively.

	Our work	Ref. [35]	Ref. [36]	Ref. [37]	Ref. [38]	Ref. [39]	Ref. [40]	Ref. [41]	Ref. [42]	Ref. [43]	Ref. [44]
$\mathcal{R}/(q_m Q_\mu)$	1.849	1.32	< 1.3	—	1.5316	0.49	0.39	1.63	2.05	1.139	0.7994
$e_\mu$	0.60%	4%	—	14.1%	3.79%	21.2%	14%	3%	10.5%	8.8%	9.3%
$d$	4	4	4	4	4	10	4	4	7	4	3
Basis	Spin-OAM	Spin-OAM	OAM	Spin-OAM	OAM	OAM	Spin-OAM	Spin-OAM	OAM	OAM	OAM
Source	WCS	PPKTP	BBO	WCS	BBO	PPKTP	PPKTP	WCS	WCS	BBO	BBO
Channel	Table	Table	Table	1.2 km	Table	Table	300 m	Table	Table	Table	Table

communication channels vary from one to one. However, Table II gives a clear picture of some key indexes (such as the QBER and secret key rate) and shows the relative merits of different systems.

## V. CONCLUSION

In conclusion, we propose and verify the feasibility of a four-dimensional QKD protocol by utilizing the nonseparable feature of the vector vortex and the polarization-OAM interconversion ability of the  $q$  plate. The characterization experiment achieves a very low QBER and experimental error. The SKRPSS is as high as  $1.849 \pm 0.008$  bits with a weak coherent light source. Our work enhances the performance quality of HDQKD with polarization-OAM hybrid states. The no-interferometric and precise preparation and measurement methods are ready for practical HDQKD systems. Furthermore, our work also reveals that HD quantum state manipulation can be simplified in some important scenarios by utilizing the nonseparable feature of vector vortex photons.

## ACKNOWLEDGMENTS

The authors acknowledge Martin P. J. Lavery for fruitful discussion. This work has been supported by the National Key Research And Development Program of China (Grants No. 2016YFA0302600); the National Natural Science Foundation of China (Grants No. 61627820, No. 61775207, No. 61675189, No. 61622506, No. 61475148, and No. 61575183); and the Anhui Initiative in Quantum Information Technologies.

- [1] G. Milione, H. I. Sztul, D. A. Nolan, and R. R. Alfano, Higher-Order Poincaré Sphere, Stokes Parameters, and the Angular Momentum of Light, *Phys. Rev. Lett.* **107**, 053601 (2011).
- [2] G. Milione, S. Evans, D. A. Nolan, and R. R. Alfano, Higher Order Pancharatnam-Berry Phase and the Angular Momentum of Light Giovanni, *Phys. Rev. Lett.* **108**, 190401 (2012).
- [3] L. Allen, M. W. Beijersbergen, R. J. C. Spreeuw, and J. P. Woerdman, Orbital angular momentum of light and the transformation of Laguerre-Gaussian laser modes, *Phys. Rev. A* **45**, 8185 (1992).
- [4] M. Erhard, R. Fickler, M. Krenn, and A. Zeilinger, Twisted photons: New quantum perspectives in high dimensions, *Light Sci. Appl.* **7**, 17146 (2018).
- [5] D. G. Hall, Vector-beam solutions of Maxwell's wave equation Dennis, *Opt. Lett.* **21**, 9 (1996).
- [6] C. Maurer, A. Jesacher, S. Fürhapter, S. Bernet, and M. Ritsch-Marte, Tailoring of arbitrary optical vector beams, *New J. Phys.* **9**, 78 (2007).
- [7] Q. Zhan, Cylindrical vector beams: From mathematical concepts to applications, *Adv. Opt. Photonics* **1**, 1 (2009).
- [8] A. Holleczek, A. Aiello, C. Gabriel, C. Marquardt, and G. Leuchs, Classical and quantum properties of cylindrically polarized states of light, *Opt. Express* **19**, 9714 (2011).
- [9] D. Naidoo, F. S. Roux, A. Dudley, I. Litvin, B. Piccirillo, L. Marrucci, and A. Forbes, Controlled generation of higher-order Poincaré sphere beams from a laser, *Nat. Photonics* **10**, 327 (2016).
- [10] M. J. Padgett and J. Courtial, Poincaré-sphere equivalent for light beams containing orbital angular momentum, *Opt. Lett.* **24**, 430 (1999).
- [11] R. Fickler, G. Campbell, B. Buchler, P. K. Lam, and A. Zeilinger, Twisted light transmission over 143 km, *Proc. Natl. Acad. Sci.* **113**, 13648 (2016).
- [12] J. Wang, J.-Y. Yang, I. M. Fazal, N. Ahmed, Y. Yan, H. Huang, Y. Ren, Y. Yue, S. Dolinar, M. Tur, and A. E. Willner, Terabit free-space data transmission employing orbital angular momentum multiplexing, *Nat. Photonics* **6**, 488 (2012).
- [13] N. Bozinovic, Y. Yue, Y. Ren, M. Tur, P. Kristensen, H. Huang, A. E. Willner, and S. Ramachandran, Terabit-scale orbital angular momentum mode division multiplexing in fibers, *Science* **340**, 1545 (2013).
- [14] A. E. Willner, H. Huang, Y. Yan, Y. Ren, N. Ahmed, G. Xie, C. Bao, L. Li, Y. Cao, Z. Zhao, J. Wang, M. P. J. Lavery, M. Tur, S. Ramachandran, A. F. Molisch, N. Ashrafi, and S. Ashrafi, Optical communications using orbital angular momentum beams, *Adv. Opt. Photonics* **7**, 66 (2015).
- [15] G. Milione, T. A. Nguyen, J. Leach, D. A. Nolan, and R. R. Alfano, Using the nonseparability of vector beams to encode information for optical communication, *Opt. Lett.* **40**, 4887 (2015).
- [16] P. Gregg, P. Kristensen, and S. Ramachandran, Conservation of orbital angular momentum in air-core optical fibers, *Optica* **2**, 267 (2015).
- [17] G. Zhu, Y. Chen, Y. Liu, Y. Zhang, and S. Yu, Characterizing a  $14 \times 14$  OAM mode transfer matrix of a ring-core fiber based on quadrature phase-shift interference, *Opt. Lett.* **42**, 1257 (2017).
- [18] A. Wang, L. Zhu, L. Wang, J. Ai, S. Chen, and J. Wang, Directly using 8.8-km conventional multi-mode fiber for 6-mode orbital angular momentum multiplexing transmission, *Opt. Express* **26**, 10038 (2018).
- [19] A. M. Yao and M. J. Padgett, Orbital angular momentum: Origins, behavior and applications, *Adv. Opt. Photonics* **3**, 161 (2011).
- [20] R. Fickler, R. Lapkiewicz, W. N. Plick, M. Krenn, C. Schaeff, S. Ramelow, and A. Zeilinger, Quantum entanglement of high angular momenta, *Science* **338**, 640 (2012).
- [21] D. Ding, W. Zhang, S. Shi, Z. Zhou, Y. Li, B. Shi, and G. Guo, High-dimensional entanglement between distant atomic-ensemble memories, *Light Sci. Appl.* **5**, e16157 (2016).
- [22] X.-L. Wang, X.-D. Cai, Z.-E. Su, M.-C. Chen, D. Wu, L. Li, N.-L. Liu, C.-Y. Lu, and J.-W. Pan, Quantum teleportation of multiple degrees of freedom of a single photon, *Nature* **518**, 516 (2015).
- [23] V. D'Ambrosio, E. Nagali, S. P. Walborn, L. Aolita, S. Slussarenko, L. Marrucci, and F. Sciarrino, Complete experimental toolbox for alignment-free quantum communication, *Nat. Commun.* **3**, 961 (2012).

- [24] G. Vallone, V. D'Ambrosio, A. Sponselli, S. Slussarenko, L. Marrucci, F. Sciarrino, and P. Villoresi, Free-Space Quantum Key Distribution by Rotation-Invariant Twisted Photons, *Phys. Rev. Lett.* **113**, 060503 (2014).
- [25] C. H. Bennett and G. Brassard, in *Proceedings of IEEE International Conference on Computers, Systems and Signal Processing* (IEEE, New York, 1984), p. 175.
- [26] V. Scarani, H. Bechmann-Pasquinucci, N. J. Cerf, M. Dušek, N. Lütkenhaus, and M. Peev, The security of practical quantum key distribution, *Rev. Mod. Phys.* **81**, 1301 (2009).
- [27] X.-B. Wang, Beating the Photon-Number-Splitting Attack in Practical Quantum Cryptography, *Phys. Rev. Lett.* **94**, 230503 (2005).
- [28] H.-K. Lo, X. Ma, and K. Chen, Decoy State Quantum Key Distribution, *Phys. Rev. Lett.* **94**, 230504 (2005).
- [29] H.-K. Lo, M. Curty, and B. Qi, Measurement-Device-Independent Quantum Key Distribution, *Phys. Rev. Lett.* **108**, 130503 (2012).
- [30] T. Sasaki, Y. Yamamoto, and M. Koashi, Practical quantum key distribution protocol without monitoring signal disturbance, *Nature* **509**, 475 (2014).
- [31] M. Lucamarini, Z. L. Yuan, J. F. Dynes, and A. J. Shields, Overcoming the rate-distance limit of quantum key distribution without quantum repeaters, *Nature* **557**, 400 (2018).
- [32] N. J. Cerf, M. Bourennane, A. Karlsson, and N. Gisin, Security of Quantum Key Distribution Using d-Level Systems, *Phys. Rev. Lett.* **88**, 127902 (2002).
- [33] L. Sheridan and V. Scarani, Security proof for quantum key distribution using qudit systems Lana, *Phys. Rev. A* **82**, 030301(R) (2010).
- [34] K. Bradler, M. Mirhosseini, R. Fickler, A. Broadbent, and R. Boyd, Finite-key security analysis for multilevel quantum key distribution, *New J. Phys.* **18**, 073030 (2016).
- [35] I. Nape, E. Otte, A. Valles, C. Rosales-Guzmán, F. Cardano, C. Denz, and A. Forbes, Self-healing high-dimensional quantum key distribution using hybrid spin-orbit Bessel states, *Opt. Express* **26**, 26946 (2018).
- [36] F. Bouchard, F. Hufnagel, D. Koutny, A. Abbas, A. Sit, K. Heshami, R. Fickler, and E. Karimi, Full characterization of a high-dimensional quantum communication channel, arXiv:1806.08018 (2018).
- [37] D. Cozzolino, D. Bacco, B. Da Lio, K. Ingerslev, Y. Ding, K. Dalgaard, P. Kristensen, M. Galili, K. Rottwitt, S. Ramachandran, and L. K. Oxenlowe, Fiber based high-dimensional quantum communication with twisted photons, arXiv:1803.10138 (2018).
- [38] F. Bouchard, K. Heshami, D. England, R. Fickler, R. W. Boyd, B.-G. Englert, L. L. Sánchez-Soto, and E. Karimi, Experimental investigation of quantum key distribution protocols with twisted photons, arXiv:1802.05773 (2018).
- [39] H. Larocque, J. Gagnon-Bischoff, D. Mortimer, Y. Zhang, F. Bouchard, J. Upham, V. Grillo, R. W. Boyd, and E. Karimi, Generalized optical angular momentum sorter and its application to high-dimensional quantum cryptography, *Opt. Express* **25**, 19832 (2017).
- [40] A. Sit, F. Bouchard, R. Fickler, J. Gagnon-Bischoff, H. Larocque, K. Heshami, D. Elser, C. Peuntinger, K. Gunthner, B. Heim, C. Marquardt, G. Leuchs, R. W. Boyd, and E. Karimi, High-dimensional intracity quantum cryptography with structured photons, *Optica* **4**, 1006 (2017).
- [41] B. Ndagano, I. Nape, B. Perez-Garcia, S. Scholes, R. I. Hernandez-Aranda, T. Konrad, M. P. J. Lavery, and A. Forbes, A deterministic detector for vector vortex states, *Sci. Rep.* **7**, 13882 (2017).
- [42] M. Mirhosseini, O. S. Magaña-Loaiza, M. N. O'Sullivan, B. Rodenburg, M. Malik, M. P. J. Lavery, M. J. Padgett, D. J. Gauthier, and R. W. Boyd, High-dimensional quantum cryptography with twisted light, *New J. Phys.* **17**, 033033 (2015).
- [43] M. Mafu, A. Dudley, S. Goyal, D. Giovannini, M. McLaren, M. J. Padgett, T. Konrad, F. Petruccione, N. Lütkenhaus, and A. Forbes, Higher-dimensional orbital-angular-momentum-based quantum key distribution with mutually unbiased bases, *Phys. Rev. A – At. Mol. Opt. Phys.* **88**, 032305 (2013).
- [44] S. Gröblacher, T. Jennewein, A. Vaziri, G. Weihs, and A. Zeilinger, Experimental quantum cryptography with qutrits, *New J. Phys.* **8**, 75 (2006).
- [45] S. M. H. Rafsanjani, M. Mirhosseini, O. S. Magaña-Loaiza, and R. W. Boyd, State transfer based on classical nonseparability, *Phys. Rev. A* **92**, 023827 (2015).
- [46] L. Marrucci, C. Manzo, and D. Paparo, Optical Spin-to-Orbital Angular Momentum Conversion in Inhomogeneous Anisotropic Media, *Phys. Rev. Lett.* **96**, 163905 (2006).
- [47] E. Nagali, F. Sciarrino, F. De Martini, L. Marrucci, B. Piccirillo, E. Karimi, and E. Santamato, Quantum Information Transfer from Spin to Orbital Angular Momentum of Photons, *Phys. Rev. Lett.* **103**, 013601 (2009).
- [48] L. Marrucci, E. Karimi, S. Slussarenko, B. Piccirillo, E. Santamato, E. Nagali, and F. Sciarrino, Spin-to-orbital conversion of the angular momentum of light and its classical and quantum applications, *J. Opt.* **13**, 064001 (2011).
- [49] V. D'Ambrosio, N. Spagnolo, L. Del Re, S. Slussarenko, Y. Li, L. C. Kwek, L. Marrucci, S. P. Walborn, L. Aolita, and F. Sciarrino, Photonic polarization gears for ultra-sensitive angular measurements, *Nat. Commun.* **4**, 2432 (2013).
- [50] X. Ma, B. Qi, Y. Zhao, and H.-K. Lo, Practical decoy state for quantum key distribution, *Phys. Rev. A* **72**, 012326 (2005).
- [51] D. Gottesman, H.-K. Lo, N. Lütkenhaus, and J. Preskill, Security of quantum key distribution with imperfect devices Daniel, *Quantum Inf. Comput.* **4**, 325 (2004).
- [52] Y. Chen, J. Gao, Z.-Q. Jiao, K. Sun, W.-G. Shen, L.-F. Qiao, H. Tang, X.-F. Lin, and X.-M. Jin, Mapping Twisted Light into and out of a Photonic Chip, *Phys. Rev. Lett.* **121**, 233602 (2018).
- [53] S. F. Mousavi, R. Nouroozi, G. Vallone, and P. Villoresi, Integrated optical modulator manipulating the polarization and rotation handedness of orbital angular momentum states, *Sci. Rep.* **7**, 3835 (2017).
- [54] S. F. Mousavi, G. Vallone, P. Villoresi, and R. Nouroozi, Generation of mutually unbiased bases for 4D-QKD with structured photons via LNOI photonic wire, *J. Opt.* **20**, 095802 (2018).
- [55] G. Gibson, J. Courtial, M. J. Padgett, M. Vasnetsov, V. Pas'ko, S. Barnett, and S. Franke-Arnold, Free-space information transfer using light beams carrying orbital angular momentum, *Opt. Express* **12**, 5448 (2004).

- [56] J. Leach, M. J. Padgett, S. M. Barnett, S. Franke-Arnold, and J. Courtial, Measuring the Orbital Angular Momentum of a Single Photon, *Phys. Rev. Lett.* **88**, 257901 (2002).
- [57] J. Leach, J. Courtial, K. Skeldon, S. M. Barnett, S. Franke-Arnold, and M. J. Padgett, Interferometric Methods to Measure Orbital and Spin, or the Total Angular Momentum of a Single Photon, *Phys. Rev. Lett.* **92**, 013601 (2004).
- [58] G. C. G. Berkhout, M. P. J. Lavery, J. Courtial, M. W. Beijersbergen, and M. J. Padgett, Efficient Sorting of Orbital Angular Momentum States of Light, *Phys. Rev. Lett.* **105**, 153601 (2010).
- [59] M. N. O'Sullivan, M. Mirhosseini, M. Malik, and R. W. Boyd, Near-perfect sorting of orbital angular momentum and angular position states of light, *Opt. Express* **20**, 24444 (2012).
- [60] M. Mirhosseini, M. Malik, Z. Shi, and R. W. Boyd, Efficient separation of the orbital angular momentum eigenstates of light, *Nat. Commun.* **4**, 2781 (2013).
- [61] Y. Wen, I. Chremmos, Y. Chen, J. Zhu, Y. Zhang, and S. Yu, Spiral Transformation for High-Resolution and Efficient Sorting of Optical Vortex Modes, *Phys. Rev. Lett.* **120**, 193904 (2018).
- [62] B. Ndagano, I. Nape, M. A. Cox, C. Rosales-Guzman, and A. Forbes, Creation and detection of vector vortex modes for classical and quantum communication, *J. Light. Technol.* **36**, 292 (2018).